Molecular Physics, Vol. 103, No. 13, 10 July 2005, 1837–1846

Taylor & Francis
Taylor & Francis Group

Correlated energy disposal and scattering dynamics of the $Cl + CD_4(\nu_3 = 2)$ reaction

HANS A. BECHTEL†, ZEE HWAN KIM‡, JON P. CAMDEN and RICHARD N. ZARE*

Department of Chemistry, Stanford University Stanford, California 94305-5080, USA

(*Received 19 November 2004; in final form 16 December 2004*)

Molecular chlorine, methane and helium are co-expanded into the extraction region of a Wiley–McLaren time-of-flight spectrometer. After preparing the first overtone of the antisymmetric stretch ($\nu_3 = 2$) with direct IR excitation, the reaction is initiated by photolysing Cl_2 with 355 nm light to produce mono-energetic Cl atoms with a translational energy of 0.18 eV. The CD_3 and DCl products are state-selectively detected via resonance enhanced multiphoton ionization (REMPI) and analysed with the core-extraction technique. Unusual structure in the $3p_z$ CD_3 REMPI spectrum suggests the presence of a previously unobserved transition, which we assign to the stretch–bend combination ($1^1_1 2^1_1$) band. The product correlated energy disposal and the scattering distributions are compared with the same quantities for the $Cl + CH_4(\nu_3 = 2)$ reaction and found to be similar, although subtle differences are observed. The results for the $Cl + CD_4(\nu_3 = 2)$ reaction support a localized chemistry model in which the Cl atom interacts with a single C–D oscillator and leaves the CD_3 methyl radical as a spectator.

1. Introduction

Excitation of different vibrational motions in polyatomic molecules can have profound effects on chemical reactions, causing changes in reactivity or alterations in the major product channels. The groups of Crim [1, 2] and Zare [3–5] first demonstrated that vibrational excitation can lead to bond- and mode-selectivity in the $H + HOD$ reaction, where excitation of the O–H stretch in HOD selectively enhanced the hydrogen-abstraction channel and excitation of the O–D stretch enhanced the deuterium-abstraction channel. Since these early experiments, vibrational control has been achieved in a number of reaction systems [6–8], including the $Cl + CH_4$ reaction [9–17]. Recently, Zare and co-workers [14, 16] demonstrated that methane prepared in the local mode $|1100\rangle$, where one quantum of stretch excitation is placed in two C–H oscillators, reacts differently than methane prepared in the local mode $|2000\rangle$, where two quanta of stretch excitation are placed in one C–H oscillator.

In this article, we present the correlated energy disposal and channel-specific angular distributions of the products from the $Cl + CD_4(\nu_3 = 2)$ reaction and make a detailed comparison with similar information from the $Cl + CH_4(\nu_3 = 2)$ reaction, examined previously by Kim *et al.* [15]. The vibrational motion of the $\nu_3 = 2$ vibration in CH_4 and CD_4 is nominally the same in that both correlate to the local mode $|1100, F_2\rangle$, but deuteration shifts the vibrational frequency from 6000 cm^{-1} in CH_4 to 4500 cm^{-1} in CD_4. Although the $Cl + CD_4(\nu_3 = 2)$ reaction has substantially less energy available to the products at similar collision energies, deuteration also scales the vibrational spacings of the products by a comparable factor. Thus, we expect the two vibrationally excited reactions to behave similarly. Our results support this supposition, but also indicate that subtle differences exist between the dynamics of the $Cl + CH_4(\nu_3 = 2)$ and $Cl + CD_4(\nu_3 = 2)$ reactions.

2. Energetics and experimental procedures

Figure 1 displays the relevant energetics of the $Cl + CH_4 \rightarrow HCl + CH_3$ and $Cl + CD_4 \rightarrow DCl + CD_3$ reactions. The $Cl + CH_4$ reaction is slightly endothermic [19], $\Delta H = 600\,cm^{-1}$ (1.7 kcal mol^{-1}), and has an activation barrier in the 800–1300 cm^{-1} (2.4–3.6 kcal mol^{-1}) or 1300–1900 cm^{-1} (3.6–5.5 kcal mol^{-1}) range, based on experimental [20] or *ab initio* calculations [21],

* Corresponding author. Email: zare@stanford.edu
†Present address. Department of Chemistry, Massachusetts Institute of Technology, 77 Massachusetts Ave, 6-022, Cambridge, MA 02139, USA.
‡Present address. Department of Chemistry, University of California Berkeley, Berkeley, California 94720-1460, USA.

Molecular Physics
ISSN 0026–8976 print/ISSN 1362–3028 online
http://www.tandf.co.uk/journals
DOI: 10.1080/00268970500044814

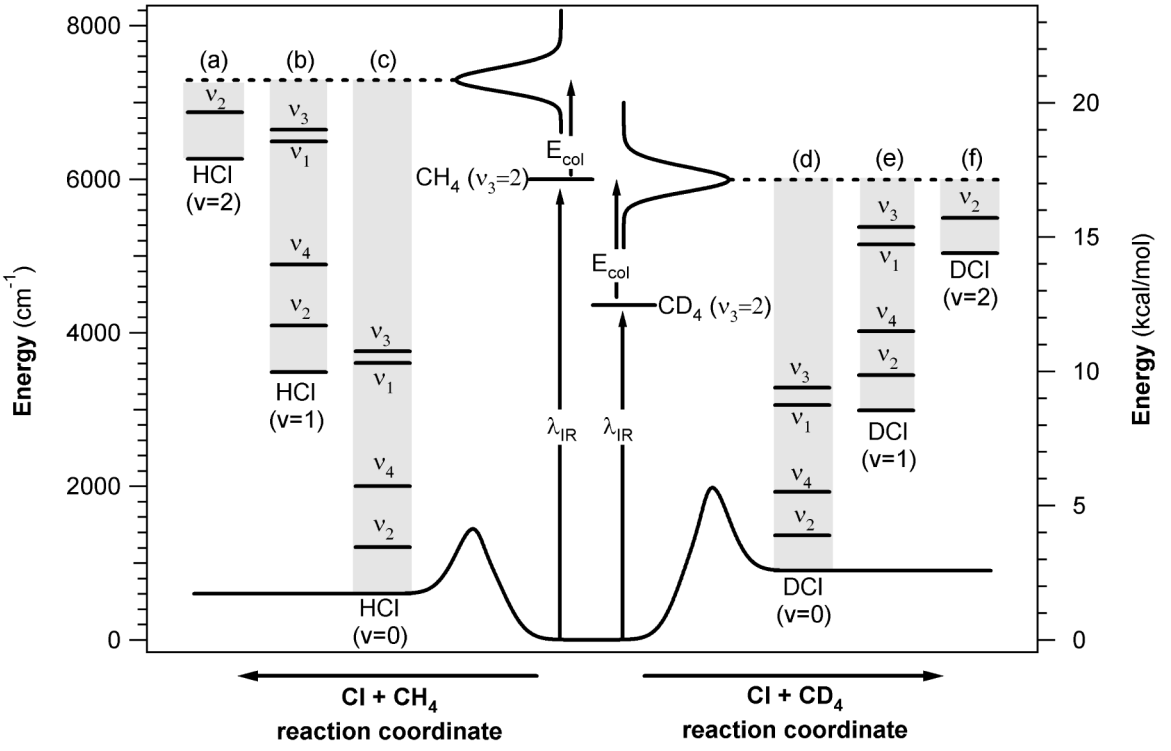

Figure 1. Energetics of the $Cl + CH_4(\nu_3 = 2)$ and $Cl + CD_4(\nu_3 = 2)$ reactions. Channels (a), (b) and (c) correspond to the production of $HCl(v = 2)$, $HCl(v = 1)$ and $HCl(v = 0)$, respectively, with varying degrees of CH_3 excitation. Likewise, channels (d), (e) and (f) correspond to the production of $DCl(v = 0)$, $DCl(v = 1)$ and $DCl(v = 2)$, respectively, with varying degrees of CD_3 excitation. The CH_3/CD_3 vibrational modes are the symmetric stretch ($\nu_1 = 3004/2158\,cm^{-1}$), the umbrella bend ($\nu_2 = 610/458\,cm^{-1}$), the antisymmetric stretch ($\nu_3 = 3160/2381\,cm^{-1}$) and the deformation ($\nu_4 = 1400/1027\,cm^{-1}$). The collision energy distributions are determined from the formulas of van der Zande *et al.* [18], assuming a translational temperature of 10 K.

respectively. The barrier is overcome by a combination of translational and vibrational energy: photolysis of Cl_2 at 355 nm provides $1290 \pm 140\,cm^{-1}$ (0.16 ± 0.02 eV) of translational energy in the centre-of-mass frame, and excitation of the antisymmetric stretch overtone ($\nu_3 = 2$) provides $\sim 6000\,cm^{-1}$ of vibrational energy. The $Cl + CD_4$ reaction is slightly more endothermic because of zero point energy effects, $\Delta H = 900\,cm^{-1}$ ($2.6\,kcal\,mol^{-1}$). The *ab initio* barrier height is $\sim 2200\,cm^{-1}$ ($6.4\,kcal\,mol^{-1}$) [21]. Photolysis of Cl_2 at 355 nm provides $1490 \pm 150\,cm^{-1}$ (0.18 ± 0.02 eV) of translational energy in the centre-of-mass frame, and excitation of the antisymmetric stretch overtone ($\nu_3 = 2$) provides $\sim 4500\,cm^{-1}$ of vibrational energy. Figure 1 also displays the energetically allowed vibrational states of the products. For the $Cl + CH_4$ and $Cl + CD_4$ reactions, the total energy, ~ 7300 and $\sim 6000\,cm^{-1}$, respectively, is enough to populate both HCl/DCl($v = 1$) and HCl/DCl($v = 2$) vibrational levels.

The methods and experimental apparatus have been described in detail previously [10, 22]; therefore, only the primary features are presented here. A 1:4:9 mixture of molecular chlorine (Matheson, research grade, 99.999%), methane (CD_4: Cambridge, 98%) and helium (Liquid Carbonic, 99.995%) is supersonically expanded into the extraction region of a Wiley–McLaren time-of-flight (TOF) spectrometer [23]. The vibrational state of methane is prepared by direct IR excitation. The reaction is initiated by the photolysis of Cl_2 with linearly polarized 355 nm light, which produces mono-energetic Cl atoms primarily in the ground state ($^2P_{3/2}$) with an anisotropy parameter $\beta = -1$ [24]. After a delay between 20 and 80 ns, the products are state selectively ionized by $2 + 1$ resonance-enhanced multiphoton ionization (REMPI), separated by mass, and detected by microchannel plates. The reactive signal from vibrationally excited methane is separated from backgrounds by modulating the IR light and subtracting the resultant signals on a shot-by-shot basis.

The IR radiation required to excite the antisymmetric stretch overtone of $CD_4(\nu_3 = 2)$ is generated in a two-step process involving difference-frequency generation and optical parametric amplification. Mid-IR light at $\lambda = 2.2\,\mu m$ is first generated via difference-frequency

generation by combining the 1.064 μm fundamental of a Nd:YAG laser (Continuum PL9020) with the output of a dye laser (Continuum ND6000, Exciton LDS 751) in a lithium niobate ($LiNbO_3$) crystal. The mid-IR radiation is then parametrically amplified in a second $LiNbO_3$ crystal that is pumped by another 1.064 μm beam to produce approximately 15 mJ of the 2.2 μm light.

The photolysis light is generated from the third harmonic of a Nd^{3+}:YAG laser (Continuum PL9020) and the probe light for REMPI is generated by frequency doubling the fundamental of a dye laser output (Quanta Ray DCR-2A, Lambda Physik FL 2002, Exciton LD 489 or DCM/LDS 698) in a BBO crystal. The DCl products are detected via the F $^1\Delta_2$–X $^1\Sigma^+(0,0)$ and F $^1\Delta_2$–X $^1\Sigma^+(1,1)$ transitions [25, 26], and the methyl radical products are detected by the $3p_z$ $^2A_2''$–X $^2A_2''$ transition [27]. Approximately 2 mJ of ~240 nm light are used to probe the DCl products and less than 1.5 mJ of ~330 nm light are used to probe the CD_3 products. All lasers are focused into the chamber using separate $f = 50$ cm lenses.

A photoelastic modulator (PEM-80, Hinds International Inc.) flips the direction of the photolysis laser polarization between parallel and perpendicular to the TOF axis on an every-other-shot basis in order to obtain the isotropic $I_{iso} = I_{\parallel} + 2I_{\perp}$ and anisotropic $I_{aniso} = 2(I_{\parallel} - I_{\perp})$ components of the core-extracted TOF profiles. The isotropic TOF profile removes any dependence on the photolysis spatial anisotropy and thus provides a direct measurement of the speed distribution. With knowledge of the internal energy of the co-products, these profiles can be analysed and converted into differential cross-sections (DCSs) by a method similar to that of Simpson *et al*. [10]. The anisotropic TOF profiles are analysed to estimate the amount of internal energy deposited into the co-product by a method described in previous publications [15, 22].

3. Results

3.1. *CH_3/CD_3 product state distributions*

Figure 2 shows the CH_3 and CD_3 REMPI spectra from the $Cl + CH_4(\nu_3 = 2)$ and $Cl + CD_4(\nu_3 = 2)$ reactions. The dominant feature in both spectra is the presence of the 1_1^1 band, showing that methyl radicals are produced with symmetric stretch excitation. Based on this large intensity, we believe excitation of the methyl radical symmetric stretch represents a dominant channel in both the $Cl + CH_4(\nu_3 = 2)$ and $Cl + CD_4(\nu_3 = 2)$ reactions. The most striking difference between the CH_3 and CD_3

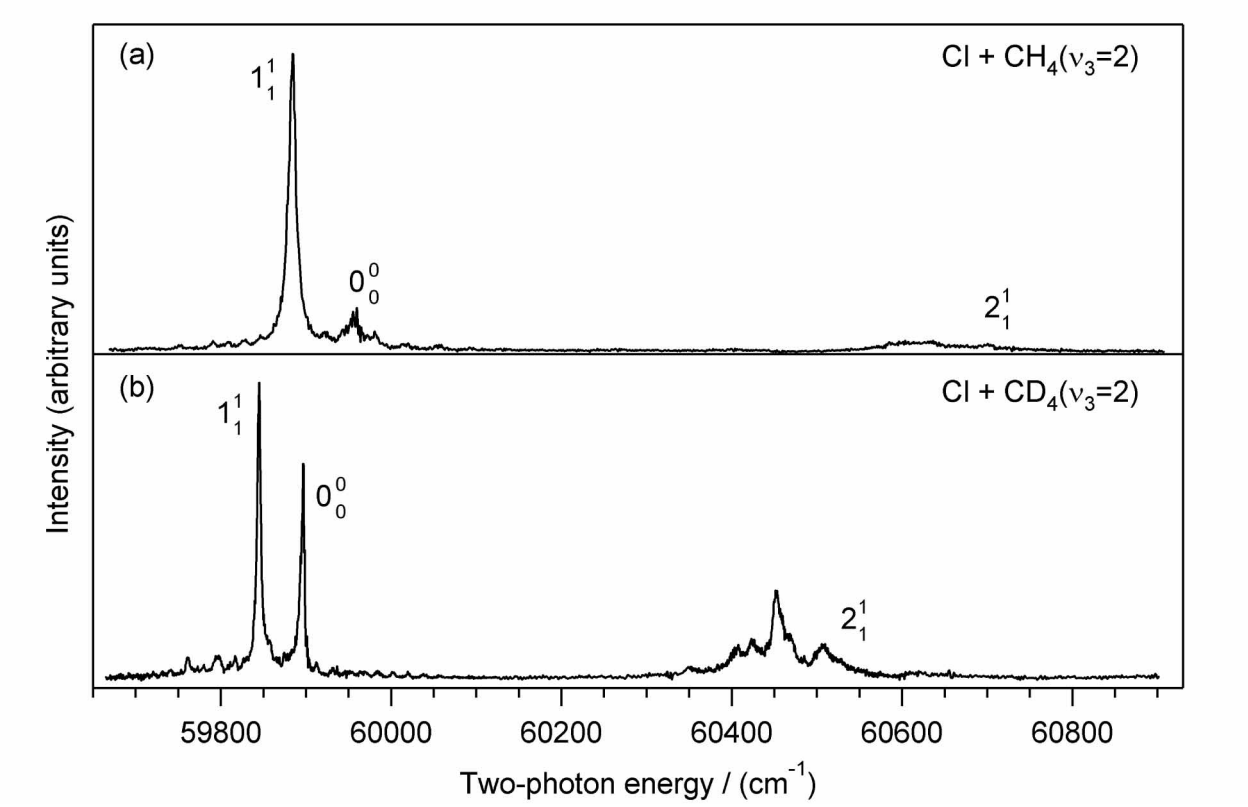

Figure 2. 2+1 REMPI spectrum of the (*a*) CH_3 and (*b*) CD_3 products from the $Cl + CH_4(\nu_3 = 2)$ and $Cl + CD_4(\nu_3 = 2)$ reactions.

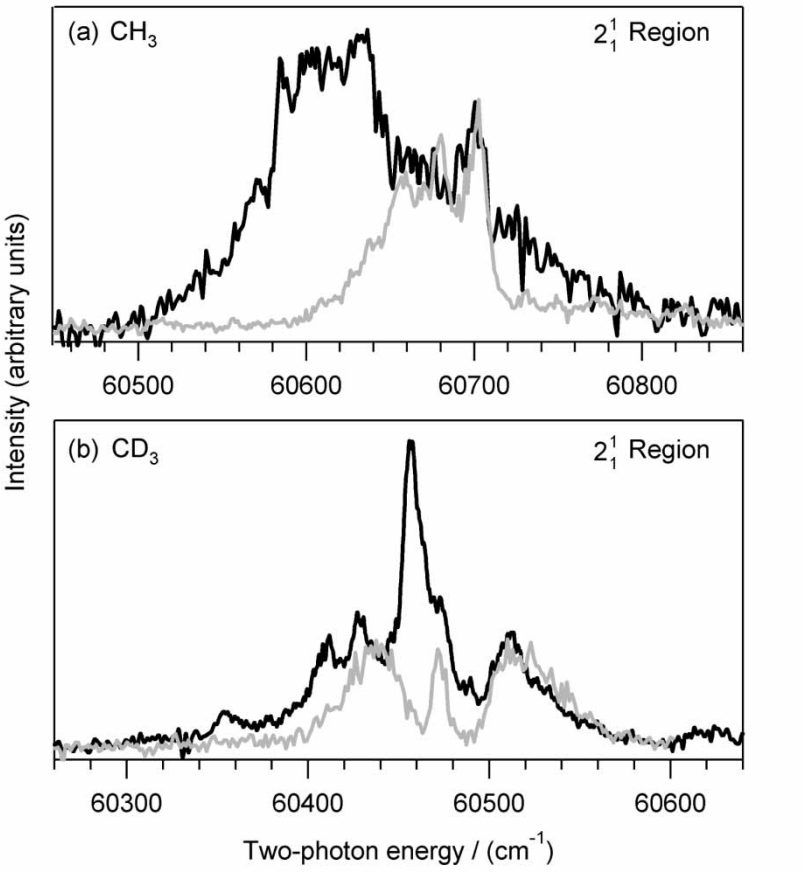

Figure 3. (*a*) 2_1^1 region of the 2+1 REMPI spectrum of the CH_3 products from the $Cl + CH_4(\nu_3 = 2)$ reaction, black line, and the $Cl + CH_4(\nu_3 = 1)$ reaction, grey line. (*b*) 2_1^1 region of the 2+1 REMPI spectrum of the CD_3 products from the $Cl + CD_4(\nu_3 = 2)$ reaction, black line, and the $Cl + CHD_3(\nu_1 = 1)$ reaction, grey line.

REMPI spectra, however, is the change in relative intensities of the 1_1^1 and 0_0^0 bands: the $Cl + CH_4(\nu_3 = 2)$ reaction produces a negligible amount of the CH_3 0_0^0 band as compared to the 1_1^1 band, whereas the $Cl + CD_4(\nu_3 = 2)$ reaction produces comparable amounts of the CD_3 0_0^0 and 1_1^1 bands. Recent *ab initio* calculations of Mebel and co-workers [28, 29] indicate that the Franck–Condon factors for the 0_0^0 and 1_1^1 bands are nearly identical for CH_3 and differ by less than 10% in CD_3. This 10% loss of sensitivity for the 1_1^1 band in CD_3 is clearly not enough to account for the intensity differences between CH_3 and CD_3 in the 1_1^1 and 0_0^0 bands. Different predissociation rates of the intermediate state in the 2+1 REMPI detection process could account for the intensity discrepancies. Because these rates are unknown, we are unable to conclude that the $Cl + CD_4(\nu_3 = 2)$ reaction produces more ground-state methyl radical than the $Cl + CH_4$ $(\nu_3 = 2)$ reaction.

Figure 2 also indicates that there is intensity in the 2_1^1 region of the CH_3 and CD_3 REMPI spectra. A detailed investigation of this region, however, shows the band shape to be dramatically different than the band shape of the 2_1^1 band observed in methyl iodide photodissociation or in the $Cl + CH_4(\nu_3 = 1)$ and $Cl + CHD_3(\nu_1 = 1)$ reactions, as shown in figure 3. Two possible sources may account for these differences in band shape for both the CH_3 and CD_3 products from the $Cl + CH_4$ $(\nu_3 = 2)$ and $Cl + CD_4(\nu_3 = 2)$ reactions: (1) a different rotational distribution of the 2_1^1 band or (2) the presence of another vibrational band. A band shape analysis of the CH_3 2_1^1 band has not been performed to our knowledge, primarily because of extensive predissociation in the upper electronic state that broadens the peaks and prevents individual rotational lines from being resolved. The CD_3 2_1^1 band, on the other hand, has been examined in greater detail because the REMPI scheme for CD_3 is substantially less predissociative. Parker *et al.* [30] examined the CD_3 2_1^1 band from CD_3I photolysis at 266 nm and identified distinctive P, Q, R and S branches, similar to the REMPI spectrum of the CD_3 products from the $Cl + CHD_3(\nu_1 = 1)$ reaction shown in figure 3. Based on their assignments and calculations of the rotational constants of the 2_1^1 band, even a dramatic

Table 1. Peak assignments of $3p_z\,^2A_2'' - X^2A_2''$ vibronic transitions.

	CH_3			CD_3		
Transition	Wavelength/nm[a]	Two-photon energy/cm^{-1}[b]	Origin shift/cm^{-1}	Wavelength/nm[a]	Two photon energy/cm^{-1}[b]	Origin shift/cm^{-1}
1_1^1	333.9	59885	−73	334.1	59845	−52
0_0^0	333.5	59958	–	333.8	59897	–
$1_1^1 2_1^1$	329.9	∼60610	652	330.7	60456[c]	559
2_1^1	329.5	60673	715	330.6	60472	575

[a]Wavelength values are reported in air.
[b]Two-photon energies are reported in vacuum. The experimental uncertainty of the Q-branch peak positions is ∼4 cm^{-1}.
[c]Experimental position of largest peak.

change in the rotational distribution is unlikely to create the band shape we observe in the CD_3 products from the Cl + $CD_4(\nu_3 = 2)$ reaction. Consequently, we believe the additional structure arises from another band rather than a different rotational distribution.

Previous assignments and the large blue shift (∼650 cm^{-1} for CH_3 and ∼560 cm^{-1} for CD_3) from the 0_0^0 band constrain the identity of the band considerably (see table 1). First, the band must originate from vibrationally excited methyl radicals because the band has not been observed from reactions that produce significant amounts of ground state methyl radical. Second, the vibrational energy of the $3p_z$ electronic state must be higher than the vibrational energy of the ground electronic state in order to obtain the necessary blue shift from the origin band. Of the four vibrational modes in CH_3 and CD_3, only the symmetric stretch (ν_1) and the umbrella bend (ν_2) have been observed in the $3p_z$ 2+1 REMPI scheme [27]. It is unlikely that the source of the additional structure in the 2_1^1 region of the spectra arises from the 3_1^1 or 4_1^1 bands because *ab initio* calculations [28] indicate that the frequencies of the antisymmetric stretch (ν_3) and the degenerate bend (ν_4) vibrations do not change significantly between the ground and the $3p_z$ electronic states. Indeed, only the umbrella bend (ν_2) changes frequency considerably between the two electronic states. The hitherto unseen intensity of the 1_1^1 band in both the CH_3 and CD_3 spectra suggests that the new band may be linked to the presence of a symmetric stretch-excited methyl radical; yet the observed blue shift is not large enough to be the 1_1^2 band. If we consider combination bands, however, the $1_1^1 2_1^1$ band becomes a likely candidate. This band, which results from methyl radicals having one quantum of excitation in the symmetric stretch and one quantum of excitation in the umbrella bend, is expected to occur in the region of the 2_1^1 band as determined by our experimental values for the 1_1^1 and 2_1^1 band. The expected blue shift of the $1_1^1 2_1^1$ band from the 0_0^0 band is 642 and 522 cm^{-1} for CH_4 and CD_4, respectively. These values are in good agreement with the observed shifts. Moreover, calculations indicate that the Franck–Condon factors of the $1_1^1 2_1^1$ band are favourable for both CH_3 and CD_3 with less than a 15% decrease in sensitivity as compared to the 0_0^0 bands [29]. Based on these arguments, we tentatively assign the additional structure in this region of the $3p_z$ REMPI spectrum to the $1_1^1 2_1^1$ band. Further experiments are necessary to determine with confidence the band origin. The spatial anisotropy measurements presented below further support this assignment. In addition, the assignment of the stretch–bend combination band in the CH_3 and CD_3 spectrum implies that the shift to the red for the 4_1^1 band in the CHD_2 REMPI spectrum from the Cl + $CH_2D_2|1100\rangle$ reaction, as observed by Bechtel *et al.* [16], may result from the $1_1^1 4_1^1$ band.

4. Energy disposal and scattering

Figure 4 shows representative isotropic $I_{iso} = I_\parallel + 2I_\perp$ and anisotropic $I_{aniso} = 2(I_\parallel - I_\perp)$ core-extracted TOF profiles of the products from the Cl + $CD_4(\nu_3 = 2)$ reactions. The DCl($v = 0$, $J = 1$) and DCl($v = 1$, $J = 1$) TOF profiles are obtained on the R(1) line of the F $^1\Delta_2$–X $^1\Sigma^+(0,0)$ and F $^1\Delta_2$–X $^1\Sigma^+(1,1)$ bands, respectively. The TOF measurements showed no dependence on rotational level within our signal-to-noise ratio. For the $CD_3(\nu_1)$ products, the TOF profile is obtained on the Q-branch of the 1_1^1 band, whereas for the CD_3 products in the 2_1^1 region, the TOF profile is obtained on the most intense peak. Accurate $CD_3(v = 0)$ TOF profiles could not be obtained because the transfer of population to the stretching states in CD_4 necessarily depletes the signal arising from the reaction of Cl with ground-state CD_4.

Figure 4 also shows the speed distributions and spatial anisotropy measurements, obtained by fitting the isotropic and anisotropic TOF profiles, as well as

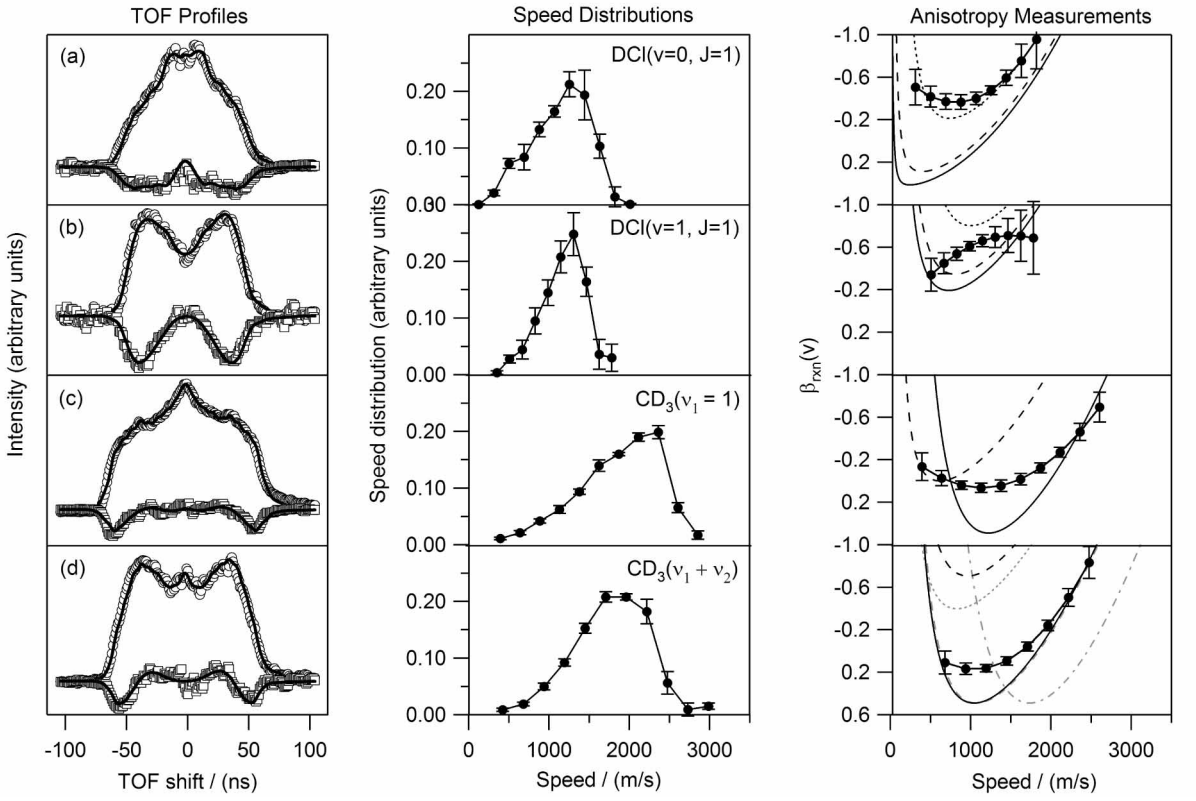

Figure 4. Isotropic (open circles) and anisotropic (open squares) TOF profiles, speed distributions and spatial anisotropy measurements of the products from the $Cl + CD_4(\nu_3 = 2)$ reaction: (*a*) DCl($v = 0$, $J = 1$), (*b*) DCl($v = 1$, $J = 1$), (*c*) $CD_3(\nu_1 = 1)$ and (*d*) $CD_3(\nu_1+\nu_2)$. For the TOF profiles, the thick, solid line is the result of the fit. For the speed-dependent spatial anisotropy measurements, the thick, solid lines with filled circles represent the experimental values and the remaining curves are calculated assuming various degrees of co-product internal energy. For the DCl($v = 0$) and DCl($v = 1$) products, the theoretical curves correspond to the expected anisotropy assuming the detected product is coincident with ground state CD_3 (solid, black line), umbrella bend excited CD_3 (dashed, black line), or stretch-excited CD_3 (dotted, black line). For the $CD_3(\nu_1 = 1)$ product, the theoretical curves correspond to the expected anisotropy assuming the detected product is coincident with DCl($v = 0$) (black, solid line) and DCl($v = 1$) (black, dashed line). For the CD_3 detected in the 2_1^1 region panels there are two sets of curves: the black curves correspond to the expected anisotropy assuming the detected product is $CD_3(\nu_1+\nu_2)$ and the coincident products are either DCl($v = 0$) (solid line) or DCl($v = 1$) (dashed line). The grey curves correspond to the expected anisotropy assuming the detected product is $CD_3(\nu_2 = 1)$ and the coincident products are DCl($v = 0$) (dash-dot line), DCl($v = 1$) (dashed line), or DCl($v = 2$) (dotted line).

calculated curves that correspond to varying levels of internal energy deposited in the co-product. For the DCl(v, J) products, the three calculated curves correspond respectively to methyl radical co-products that are formed in the ground state, formed with one quantum of umbrella bend excitation, and formed with one quantum of symmetric stretch excitation. For the $CD_3(\nu_1 = 1)$ products, the two calculated curves correspond to DCl($v = 0$) and DCl($v = 1$) co-products, respectively. Two sets of curves are shown for the methyl radical products detected in the 2_1^1 region of the CD_3 REMPI spectra. The first set, shown in grey, assumes the detected product is umbrella bend excited and the curves correspond to DCl products formed in $v = 0$, 1 or 2. The second set, shown in black, assumes the detected product is umbrella bend excited and symmetric stretch excited and the curves correspond to DCl products formed in $v = 0$, $v = 1$.

Using the calculated anisotropy curves as a guide, it appears that the DCl($v = 0$) products are formed almost exclusively with stretch-excited methyl radicals. The DCl($v = 1$) products, on the other hand, are formed with both stretch-excited methyl radicals and ground-state or umbrella-bend excited methyl radicals. The measured anisotropy for the $CD_3(\nu_1 = 1)$ products indicate that both DCl($v = 0$) and DCl($v = 1$) are formed as co-products. By using the anisotropy to decompose the measured speed distribution, we are able to determine that $20 \pm 15\%$ of the $CD_3(\nu_1 = 1)$ products are formed with DCl($v = 1$), similar to the $30 \pm 15\%$

of $CH_3(\nu_1 = 1)$ coincident with $HCl(v = 1)$ in the $Cl + CH_4(\nu_3 = 2)$ reaction. Interpreting the spatial anisotropy results for the methyl radical products detected in the 2_1^1 region of the spectrum is complicated by the unknown product state. If we assume that the detected methyl radical product is umbrella bend excited, the calculated curves indicate that most of the co-products are formed in $DCl(v = 1)$ with the rest being formed in $DCl(v = 2)$. A similar analysis of the CH_3 products from the $Cl + CH_4(\nu_3 = 2)$ reaction also indicates that most of the co-products are formed in $HCl(v = 1)$ and $HCl(v = 2)$ [15]. This result is rather surprising considering that the $HCl(v = 1)$ and $HCl(v = 2)$ channels account for only 31% of the reaction products [15]. On the other hand, if we assume that the detected methyl radical product is both stretch excited and umbrella-bend excited, the calculated curves indicate that most of the co-products are formed in $HCl(v = 0)/DCl(v = 0)$ with the rest being formed in $HCl(v = 1)/DCl(v = 1)$. We believe it is more likely that the detected methyl product state is stretch excited and umbrella-bend excited, especially considering the REMPI spectrum discussed in the previous section.

The methyl radical distributions and spatial anisotropy measurements allow us to identify three major product channels (listed in order of importance):

$$\begin{aligned} Cl + CD_4(\nu_3 = 2) & \\ &\rightarrow DCl(v = 0) + CD_3(\nu_1 = 1 \text{ or } \nu_1 + \nu_2), \quad (1\,a) \\ &\rightarrow DCl(v = 1) + CD_3(\nu_2 = 0, 1), \quad (1\,b) \\ &\rightarrow DCl(v = 1) + CD_3(\nu_1 = 1 \text{ or } \nu_1 + \nu_2). \quad (1\,c) \end{aligned}$$

These three product channels are in agreement with the three major products observed in the $Cl + CH_4(\nu_3 = 2)$ reaction [15]:

$$\begin{aligned} Cl + CH_4(\nu_3 = 2) & \\ &\rightarrow HCl(v = 0) + CH_3(\nu_1 = 1 \text{ or } \nu_1 + \nu_2), \quad (2\,a) \\ &\rightarrow HCl(v = 1) + CH_3(\nu_2 = 0, 1), \quad (2\,b) \\ &\rightarrow HCl(v = 1) + CH_3(\nu_1 = 1 \text{ or } \nu_1 + \nu_2). \quad (2\,c) \end{aligned}$$

Knowledge of the correlated energy disposal allows us to convert the measured speed distributions into channel specific DCSs. As shown in figure 5, the major channels from the $Cl + CH_4(\nu_3 = 2)$ and $Cl + CD_4(\nu_3 = 2)$ reactions have different angular distributions. The HCl/DCl products from channel (a) are largely back-scattered, whereas they are sharply side-scattered in channel (b) and slightly forward-scattered in channel (c).

In order to qualitatively describe the channel specific angular distributions of the $Cl + CH_4(\nu_3 = 2)$ reaction,

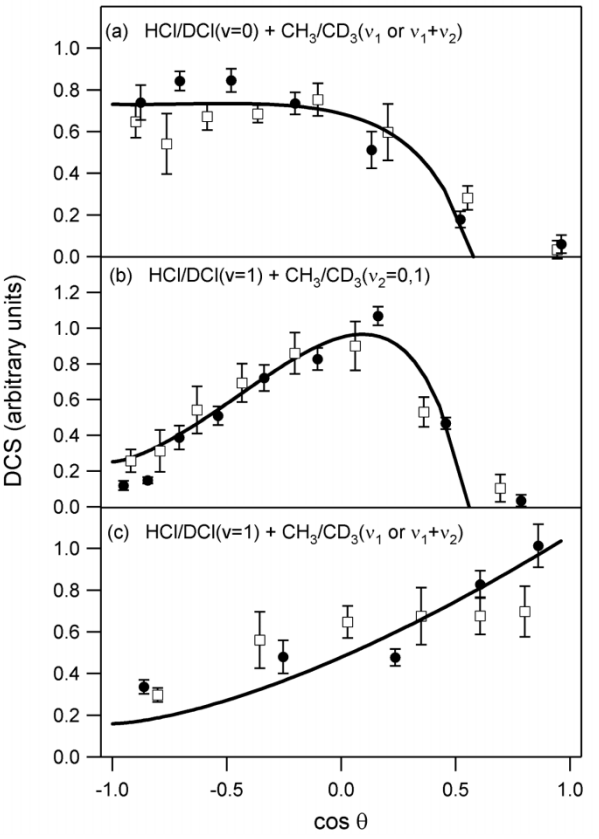

Figure 5. DCSs for the HCl/DCl products from the three major product channels of the $Cl + CH_4(\nu_3 = 2)$ and $Cl + CD_4(\nu_3 = 2)$ and reactions. The solid, closed circles represent (*a*) $HCl(v = 0) + CH_3(\nu_1 = 1 \text{ or } \nu_1+\nu_2)$, (*b*) $HCl(v = 1) + CH_3(\nu_2 = 0,1)$ and (*c*) $HCl(v = 1) + CH_3(\nu_1 = 1 \text{ or } \nu_1+\nu_2)$. The broken, open squares represent (*a*) $DCl(v = 0) + CD_3(\nu_1 = 1 \text{ or } \nu_1+\nu_2)$, (*b*) $DCl(v = 1) + CD_3(\nu_2 = 0,1)$, (*c*) $DCl(v = 1) + CD_3(\nu_1 = 1 \text{ or } \nu_1+\nu_2)$. The thick, black line shows the results of the IR-LOC model of Kim *et al.* [15]. The parameter values are discussed in the text.

Kim *et al.* [15] modified the simple hard-sphere scattering model by including an impulsive release ($\Delta E/E_0$) along the line of centres, where E_0 is the initial collision energy and ΔE is the kinetic energy release upon contact. The model assumes (1) direct, localized reactivity of the polyatomic reagent and (2) a narrow cone of acceptance around the reactive bond. The opacity function is modelled with two adjustable parameters, namely w and n. The parameter w represents the difference in reactivity between collisions at small and large impact parameters, where $w = 0$ is the maximum difference and $w = 1$ is the minimum difference. The parameter n determines how rapidly the reactivity increases at larger impact parameters. We have compared the results of this model with the DCSs from the $Cl + CH_4(\nu_3 = 2)$ and $Cl + CD_4(\nu_3 = 2)$

reactions and found them to qualitatively capture the general features of each channel (see figure 5). For the best agreement between the model and the experimental DCSs, we used the opacity function parameter $n = 3$ for all three channels and $w = 0.8$ for channel (a) and $w = 0.2$ for channels (b) and (c). For channels (a) and (b), a significant impulse release ($\Delta E/E_0 \approx 2$) causes the HCl/DCl(v) products to be deflected from their original direction, leading primarily to backward and sideward scattering. The two channels are different, however, in that the HCl/DCl($v = 1$) products favour large impact parameters ($w = 0.2$), whereas the HCl/DCl($v = 0$) products appear to have equal preference for large and small impact parameters($w = 0.8$). The sharp cut-off in the HCl/DCl($v = 1$) DCS at $\cos\theta = 0.6$ is characteristic of an impulse release at large impact parameters and is in remarkable agreement with the calculated minimum scattering angle from the model assuming the energetic maximal impulse release. For the near thermoneutral channel (c), little energy is available for an impulsive energy release. Therefore, the tendency for forward-scattering is indicative of a preference for high impact parameters.

Although the IR-LOC model is over-simplified to quantitatively describe the experimental results, the qualitative agreement supports the hypothesis that an impulse release occurs along the line of centres. This hypothesis is further supported by measurements of the product rotational alignment of the HCl($v = 1$, $J = 1$) channel [15]. Assuming that the rotational excitation is caused by the torque imparted to the HCl product at the transition state, the rotational angular momentum vector distribution should be perpendicular to the impulse release direction as well as cylindrically symmetric about the impulse release direction. Kim *et al*. [15] found models of the measured alignment moment A_0^2 to fit best when the HCl products are formed along the line of centres, rather than near the entrance or exit channels.

Discussion

The results presented above indicate that the energy disposal and scattering distributions for the $Cl + CD_4$ ($\nu_3 = 2$) and $Cl + CH_4(\nu_3 = 2)$ reactions are remarkably similar. As shown in figure 2, both reactions produce significant amounts of stretch-excited methyl radical, in contrast to the $Cl + CH_4(\nu_3 = 1)$ reaction in which the methyl radical products are only produced in the ground state or umbrella bend state. The source of this stretch excitation becomes apparent when the local mode model of overtone vibrations is considered. The $CH_4(\nu_3 = 2)$ and $CD_4(\nu_3 = 2)$ vibrations correlate to the local mode state $|1100, F_2\rangle$, where one quantum of energy is placed in two different C–H (C–D) oscillators. Halonen [31] has analysed the overtone spectrum of CH_4 using a local mode model that incorporates Fermi resonance interactions between stretching and bending vibrations, and found the $CH_4(\nu_3 = 2)$ state to be dominated by C–H stretching local mode character with only a 10% contribution from bending motions. Thus, if the Cl atom reacts with only one C–H (C–D) oscillator, then the other quantum of vibrational energy will be retained in the non-reactive bonds, leaving the methyl radical products stretch-excited. Based on simple local-normal mode correlations, this spectator model would also predict excitation of the methyl radical antisymmetric stretch (ν_3) in addition to the symmetric stretch (ν_1). Although we see no evidence of ν_3 excitation, we are unable to rule out $CH_3(\nu_3 = 1)/CD_3(\nu_3 = 1)$ products because this mode has not been observed in any methyl $2 + 1$ REMPI spectrum.

This localized picture of chemical reactivity is further supported by comparing the HCl product state distributions and angular distributions from the $Cl + CH_4$ ($\nu_3 = 2$) reaction [15] with the $Cl + CH_4(\nu_1 = 1)$ and $Cl + CH_4(\nu_3 = 1)$ reactions [10, 17]. First, the HCl($v = 0$) and HCl($v = 1$) rotational distributions and the branching ratio between HCl($v = 0$) and HCl($v = 1$) of all three reactions are remarkably similar, despite the $Cl + CH_4(\nu_3 = 2)$ reaction having $\sim 3000\,cm^{-1}$ more energy than either the $Cl + CH_4(\nu_1 = 1)$ and $Cl + CH_4(\nu_3 = 1)$ reactions (see table 2). Moreover, very little HCl($v = 2$) products are formed in the $Cl + CH_4(\nu_3 = 2)$ reaction, which energetically requires abstracting both quanta of energy. Third, the angular distributions for the HCl($v = 0$) + $CH_3(\nu_1 = 1$ or $\nu_1 + \nu_2)$ channel from the $Cl + CH_4(\nu_3 = 2)$ reaction show similar back-scattered behaviour as the HCl($v = 0$) + $CH_3(\nu_2 = 0,\ 1)$ channel from the $Cl + CH_4(\nu_1 = 1)$ and $Cl + CH_4(\nu_3 = 1)$ reactions. Finally, even the HCl($v = 1$) + $CH_3(\nu_1 = 1$ or $\nu_1 + \nu_2)$ channel from the $Cl + CH_4(\nu_3 = 2)$ reaction shows a tendency for forward scattering, which is analogous to the forward scattered behaviour of the HCl($v = 1$) + $CH_3(\nu_2 = 0)$ products from the fundamental-excited reactions.

Although most of the reaction products can be explained by the localized chemistry model, it does not explain the formation of the $CH_3(v = 0)$ and $CD_3(v = 0)$ products because their formation requires energy transfer between the two initially excited C–H (C–D) oscillators. Partial breakdown of the spectator limit has been observed in other systems, particularly Cl + HCN [32–35], where the breakdown is attributed to an intermediate complex that mediates intramolecular vibrational energy transfer. Experimental and theoretical results, however, strongly suggest that the reaction of

Table 2. Comparison of average rotational energy and fractional population for the HCl/DCl products from overtone and fundamental excited reactions.

Reaction	$\langle E_{rot}\rangle_{v=0}$ [a]	$\langle E_{rot}\rangle_{v=1}$ [a]	$\langle E_{rot}\rangle_{v=2}$ [a]	$f_{v=0}$	$f_{v=1}$ [b]	$f_{v=2}$ [b]
$Cl + CH_4(\nu_3 = 2)$ [c]	213 ± 55	79 ± 15	73 ± 30	69 ± 8	31 ± 8	< 0.1
$Cl + CD_4(\nu_3 = 2)$ [d]	83 ± 25	[f]	[g]	–	–	–
$Cl + CH_4(\nu_3 = 1)$ [e]	292 ± 93	53 ± 3	[h]	63 ± 7	37 ± 7	–
$Cl + CH_4(\nu_1 = 1)$ [e]	301 ± 95	41 ± 3	[h]	63 ± 7	37 ± 7	–

[a]Average rotational energy in cm^{-1}.
[b]Fractional population, $f_{v=0} + f_{v=1} + f_{v=2} = 100\%$.
[c]From Kim *et al*. [15].
[d]This work.
[e]From Bechtel *et al*. [17].
[f]The maximum observed rotational level is $J = 5$, but lack of calibration factors prevent an accurate calculation of $\langle E_{rot}\rangle_{v=1}$.
[g]Not detectable within signal to noise.
[h]Energetically not allowed.

chlorine atoms with methane is direct, with no indication of any complex formation. We believe rather that the breakdown of the spectator limit originates in the initially prepared motion of the methane reagent. Because the $\nu_3 = 2$ vibration is not a pure local mode, inter-bond coupling may be facilitated by the low-frequency bending motion associated with the stretching motion in this eigenstate. This idea is further supported by comparing correlation diagrams [36] between local mode and normal mode models of methane, which indicate that the C–D stretching vibrations of CD_4 are less localized than the C–H stretching vibrations of CH_4. Thus, the $Cl + CD_4(\nu_3 = 2)$ reaction may deviate more from the spectator model than the $Cl + CH_4(\nu_3 = 2)$ reaction, which could account for more ground state CD_3 than ground state CH_3.

Conclusions

We have measured the product state distributions, angular distributions and correlated energy disposal in the $Cl + CD_4(\nu_3 = 2)$ reaction and compared them with similar quantities from the $Cl + CH_4(\nu_3 = 2)$ reaction. The analogous scattering behaviour between the two reactions indicates that the prepared vibrational motion, not the energetics, governs the dynamics. Furthermore, the reaction is localized at a single C–H (C–D) oscillator and the methyl radical is primarily a spectator throughout the course of the reaction. The subtle differences between the $Cl + CH_4(\nu_3 = 2)$ and $Cl + CD_4(\nu_3 = 2)$ reactions, however, suggest that the spectator model is not fully sufficient to describe all the effects of overtone excitation on the reaction of atomic chlorine with methane. In the course of these studies, we identified a previously unknown hot band in the (2+1) $3p_z$ REMPI spectrum of CD_3, which we have assigned to the $1_1^1 2_1^1$ band.

Acknowledgement

The authors thank A.M. Mebel for unpublished *ab initio* calculations of Franck–Condon factors. Two of the authors (HAB and JPC) thank the National Science Foundation for graduate fellowships. HAB also acknowledges Stanford University for the award of a Stanford Graduate Fellowship. This material is based upon work supported by the National Science Foundation under Grant No. 0242103.

References

[1] A. Sinha, M.C. Hsiao, F.F. Crim. *J. chem. Phys.*, **92,** 6333 (1990).
[2] A. Sinha, M.C. Hsiao, F.F. Crim. *J. chem. Phys.*, **94,** 4928 (1991).
[3] M.J. Bronikowski, W.R. Simpson, B. Girard, R.N. Zare. *J. chem. Phys.*, **95,** 8647 (1991).
[4] M.J. Bronikowski, W.R. Simpson, R.N. Zare. *J. phys. Chem.*, **97,** 2194 (1993).
[5] M.J. Bronikowski, W.R. Simpson, R.N. Zare. *J. phys. Chem.*, **97,** 2204 (1993).
[6] F.F. Crim. *J. phys. Chem.*, **100,** 12725 (1996).
[7] R.N. Zare. *Science*, **279,** 1875 (1998).
[8] F.F. Crim. *Acc. Chem. Res.*, **32,** 877 (1999).
[9] S. Yoon, R.J. Holiday, F.F. Crim. *J. chem. Phys.*, **119,** 4755 (2003).
[10] W.R. Simpson, T.P. Rakitzis, S.A. Kandel, A.J. Orr-Ewing, R.N. Zare. *J. chem. Phys.*, **103,** 7313 (1995).
[11] W.R. Simpson, T.P. Rakitzis, S.A. Kandel, T. Levon, R.N. Zare. *J. phys. Chem.*, **100,** 7938 (1996).
[12] S. Yoon, R.J. Holiday, E.L. Silbert, F.F. Crim. *J. chem. Phys.*, **119,** 9568 (2003).

[13] S. Yoon, S. Henton, A.N. Zivkovic, F.F. Crim. *J. chem. Phys.*, **116,** 10744 (2002).
[14] Z.H. Kim, H.A. Bechtel, R.N. Zare. *J. Am. Chem. Soc.*, **123,** 12714 (2001).
[15] Z.H. Kim, H.A. Bechtel, R.N. Zare. *J. chem. Phys.*, **117,** 3232 (2002).
[16] H.A. Bechtel, Z.H. Kim, J.P. Camden, R.N. Zare. *J. chem. Phys.*, **120,** 791 (2004).
[17] H.A. Bechtel, J.P. Camden, D.J.A. Brown, R.N. Zare. *J. chem. Phys.*, **120,** 5096 (2004).
[18] W.J. van der Zande, R. Zhang, R.N. Zare, K.G. McKendrick, J.J. Valentini. *J. phys. Chem.*, **95,** 8205 (1991).
[19] R. Atkinson, D.L. Baulch, R.A. Cox, J.R.F. Hampson, J.A. Kerr, J. Troe. *J. phys. Chem. Ref. Data*, **21,** 1125 (1992).
[20] W.B. DeMore, S.P. Sander, C.J. Howard, A.R. Ravishankara, D.M. Golden, C.E. Kolb, R.F. Hampson, M.J. Kurylo, M.J. Molina. JPL Publication 97–4, Jet Propulsion Laboratory, Pasadena, CA (1997).
[21] J.C. Corchado, D.G. Truhlar, J. Espinosa-Garcia. *J. chem. Phys.*, **112,** 9375 (2000).
[22] W.R. Simpson, A.J. Orr-Ewing, T.P. Rakitzis, S.A. Kandel, R.N. Zare. *J. chem. Phys.*, **103,** 7299 (1995).
[23] W.C. Wiley, I.H. McLaren. *Rev. Sci. Instrum.*, **26,** 1150 (1955).
[24] P.C. Samartzis, B. Bakker, T.P. Rakitzis, D.H. Parker, T.N. Kitsopoulos. *J. chem. Phys.*, **110,** 5201 (1999).
[25] A. Yokoyama, T. Takayanagi. *Chem. Phys. Lett.*, **307,** 48 (1999).
[26] E.A. Rohlfing, D.W. Chandler, D.H. Parker. *J. chem. Phys.*, **87,** 5229 (1987).
[27] J.W. Hudgens, T.G. DiGiuseppe, M.C. Lin. *J. chem. Phys.*, **79,** 571 (1983).
[28] A.M. Mebel, S.-H. Lin. *Chem. Phys.*, **215,** 329 (1997).
[29] A.M. Mebel, Personal communication, 2004.
[30] D.H. Parker, Z.W. Wang, M.H.M. Janssen, D.W. Chandler. *J. chem. Phys.*, **90,** 60 (1989).
[31] L. Halonen. *J. chem. Phys.*, **106,** 831 (1997).
[32] R.B. Metz, J.M. Pfeiffer, J.D. Thoemke, F.F. Crim. *Chem. Phys. Lett.*, **221,** 347 (1994).
[33] J.M. Pfeiffer, R.B. Metz, J.D. Thoemke, E. Woods, F.F. Crim. *J. chem. Phys.*, **104,** 4490 (1996).
[34] C. Kreher, R. Theinl, K.-H. Gericke. *J. chem. Phys.*, **104,** 4481 (1996).
[35] C. Kreher, J.L. Rinnenthal, K.-H. Gericke. *J. chem. Phys.*, **108,** 3154 (1998).
[36] L. Halonen, M.S. Child. *Molec. Phys.*, **46,** 239 (1982).